Available online at www.sciencedirect.com
ScienceDirect
Trans. Nonferrous Met. Soc. China 33(2023) 2351−2364
Transactions of Nonferrous Metals Society of China
www.tnmsc.cn

Role of unusual double-peak texture in significantly enhancing cold rolling formability of AZ31 magnesium alloy sheet

Xiu-zhu HAN[1], Li HU[2], Dong-yong JIA[1], Jia-ming CHEN[2], Tao ZHOU[2], Shu-yong JIANG[3], Zheng TIAN[1]

1. Beijing Institute of Spacecraft System Engineering, Beijing 100094, China;
2. College of Materials Science and Engineering, Chongqing University of Technology, Chongqing 400054, China;
3. College of Materials Science and Engineering, Taiyuan University of Technology, Taiyuan 030024, China

Received 6 March 2022; accepted 17 June 2022

Abstract: Multi-pass cold rolling experiments were performed on AZ31 magnesium alloy sheet with unusual double-peak texture, where basal poles tilt about ±40° away from normal direction to rolling direction. This adopted sheet was fabricated by a novel technology of equal channel angular rolling and continuous bending process with subsequent annealing. Experimental results confirm that such an unusual double-peak texture contributes to a huge improvement of accumulated reduction up to 39.2%, which is over twice as much as that (18.3%) in sheet with strong basal texture. Optical microscopy and electron backscatter diffraction measurements demonstrate that the evolution of microstructure and texture in sheet with unusual double-peak texture is quite different from that in sheet with strong basal texture. Schmid factor (SF) analysis confirms that sheet with unusual double-peak texture possesses obviously large SF values for basal $\langle a \rangle$ slip and $\{10\bar{1}2\}$ extension twin (ET) and remarkably small SF values for prismatic $\langle a \rangle$ slip and pyramidal $\langle c+a \rangle$ slip during cold rolling process. Therefore, basal $\langle a \rangle$ slip and $\{10\bar{1}2\}$ ET will be activated more frequently in sheet with unusual double-peak texture to sustain plastic strain, leading to significant enhancement in cold rolling formability.

Key words: AZ31 magnesium alloy; non-basal texture; cold rolling process; microstructure evolution; deformation mechanism

1 Introduction

Under the background of lightweight design for components applied in the automotive and aerospace industries, nowadays, there exist large market demand and wide application prospect for wrought magnesium alloys, which possess low density, high specific strength and stiffness, decent damping capability and pertinent weldability [1−3]. However, the hexagonal-close packed (HCP) crystal structure of wrought magnesium alloys would result in limited slip modes during plastic deformation at room temperature (RT), which further leads to the poor RT plasticity of wrought magnesium alloys [4,5]. Moreover, the strong basal texture (*c*-axis of grains mainly concentrates towards normal direction (ND)) formed during the rolling process of fabricating sheet products has adverse effect on the plasticity of wrought magnesium alloys at RT [6,7]. Consequently, there is little doubt that the cold rolling formability, which is termed as a typical representative of plasticity at RT, is unsatisfactory for the subsequent process of wrought magnesium alloy sheets, leading to severe restriction for their practical applications.

Among these reported wrought magnesium alloys, AZ31 magnesium alloy has been termed as

Corresponding author: Li HU, Tel: +86-17358428920, E-mail: huli@cqut.edu.cn;
Dong-yong JIA, Tel: +86-13720055816, E-mail: jiadongyong163@163.com
DOI: 10.1016/S1003-6326(23)66264-8

the most widely used one at present. As the intrinsic characteristics of crystal structure can be hardly changed, tailoring the initial texture of AZ31 magnesium alloy sheet has been extensively regarded as a crucial access to enhance its plasticity at RT. Nowadays, numerous intelligent processing schemes have been proposed and conducted to tackle this issue. Some researchers are committed to reducing the intensity of basal texture in AZ31 magnesium alloy sheet. For example, HUANG et al [8] and LEE et al [9] separately introduced a weakened basal texture in AZ31 magnesium alloy sheet by differential speed rolling (DSR) and high speed rolling (HSR). By comparison, some researchers tried to introduce non-basal texture in AZ31 magnesium alloy sheet. For example, KUANG et al [10] fabricated AZ31 magnesium alloy sheet with an abnormal transverse direction (TD)-split non-basal texture via single-pass large strain electro-plastic rolling (LSER). SONG et al [11] proposed a novel technology of equal channel angular rolling and continuous bending process with subsequent annealing (ECAR−CB−A). The manufactured AZ31 magnesium alloy sheet possessed a rare RD-split non-basal texture, where basal poles tilt about ±40° away from ND to rolling direction (RD). HE et al [12] realized the texture modification of AZ31 magnesium alloy sheet by using in-plane pre-compression, pre-stretching and annealing. With this approach, an orthogonal four-peak distribution of basal texture has been introduced in the fabricated AZ31 magnesium alloy sheet. Obviously, AZ31 magnesium alloy sheets with tailored textures are continuously being fabricated with enhanced cold rolling formability. For the purpose of further broadening their engineering applications, it is of great importance to investigate the underlying mechanisms resulting in the improvement of cold rolling formability in AZ31 magnesium alloy sheet with tailored texture.

Up to date, numerous antecedent studies have been conducted on the cold rolling formability of AZ31 magnesium alloy sheets with strong basal texture. For instance, CHANG et al [13] investigated the microstructure and texture characteristics of AZ31 magnesium alloy sheet during single-pass rolling process. They found that edge cracks appeared when reduction per pass reached 22%. Similarly, LEE et al [14] reported that when AZ31 magnesium alloy sheet was rolled to an accumulated reduction of 25% in a single pass, some cracks with 2−4 mm in length were formed on the edge of the rolled sheet. Besides, HUANG et al [15] applied multi-pass cold rolling experiments on AZ31 magnesium alloy sheet. They found that AZ31 magnesium alloy sheet can be rolled to a maximum accumulated reduction (less than 25%) at small reduction per pass (less than 5%). Actually, CHUN and DAVIES et al [16] and LEE et al [17] confirmed that the texture evolution, deformed microstructure characteristics and activities of involved slip/twinning modes are closely related to the initial texture of AZ31 magnesium alloy sheet before the cold rolling process. Unfortunately, literature search demonstrates that little attention has been paid to investigating the cold rolling formability and the associated deformation mechanisms in AZ31 magnesium alloy sheet with weak basal texture, let alone for sheet with non-basal texture.

Consequently, the present study aims to specifically investigate the effect of non-basal texture on cold rolling formability of AZ31 magnesium alloy sheet. To achieve this goal, a comparative study on cold rolling formability of two kinds of sheets was performed. One sheet with a typically strong basal texture was manufactured by conventional hot rolling process and subsequent annealing treatment. By comparison, the other sheet was fabricated via ECAR−CB−A process and it possessed a RD-split non-basal texture. According to TU et al [18] and HE et al [12], the Erichsen value (an indicator of plasticity at RT) of 7.4 mm is not only larger than that of 4.2 mm in AZ31 magnesium alloy sheet with strong basal texture, but also larger than that of 5.6 mm in AZ31 magnesium alloy sheet with an orthogonal four-peak texture. This issue demonstrates a huge improvement on cold rolling formability, which is the reason for choosing the sheet with unusual double-peak texture in the present study. Afterwards, experimental investigations based on optical microscopy (OM) and electron backscatter diffraction (EBSD) measurements were synergistically performed to analyze the microstructure evolution and texture characteristics of both sheets during cold rolling process and to correlate activities of involved slip/twining modes to the superior cold rolling formability in AZ31 magnesium alloy sheet with unusual double-peak texture.

2 Experimental

In the present study, two kinds of applied AZ31 magnesium alloy sheets were 1.2 mm thick. The elemental compositions of these two sheets were consistent and shown in Table 1. Firstly, they were mechanically polished to obtain smooth surfaces on both sides. Afterwards, multi-pass cold rolling experiments were performed on these prepared sheets at a given reduction of about 10% per pass at RT. The diameter of roller was 170 mm and the roller speed was 100 mm/s. Prior to cold rolling, the sheets and rollers were all coated with graphite to guarantee a good lubricant condition. After each rolling pass, surfaces of sheets were examined carefully to determine the occurrence of cracking.

Microstructure characterization on the RD−TD plane of rolled specimen was carried out by means of Leica™ DMI5000M optical microscopy (OM). Sample preparation for OM observation consisted of mechanical grinding with 400#, 800#, 1200# and 2000# SiC papers, followed by polishing in the chosen polishing solution, which contained 1 g oxalate, 1 mL nitric acid and 98 mL H_2O. In addition, microstructure characteristics and texture evolution of rolled specimens were further investigated via EBSD measurement. The observed surface was also chosen to be RD−TD plane and the observation equipment was an FEI NOVA 400 Zeiss Sigma field emission scanning electron microscope equipped with an HKL-Nordlys MAX detector. CHEN et al [19] documented well the corresponding content about sample preparation for EBSD measurement, therefore it will not be illustrated here. In the present study, a relatively large step size of 2.6 μm was applied for these single-pass rolled samples, while a relatively minor step size of 0.5 μm was adopted for these remaining rolled samples. Finally, these EBSD data were analyzed by virtue of the Channel 5 analysis software and MTEX toolbox [20].

Table 1 Chemical composition of adopted AZ31 magnesium alloy sheets (wt.%)

Al	Zn	Mn	Fe	Si	Cu	Ni	Mg
2.88	0.86	0.30	0.0022	0.035	0.0001	0.001	Bal.

3 Results

3.1 Initial microstructure and texture of AZ31 magnesium alloy sheets

Figure 1 exhibits the initial microstructure and texture of the as-received sheets. Obviously, these

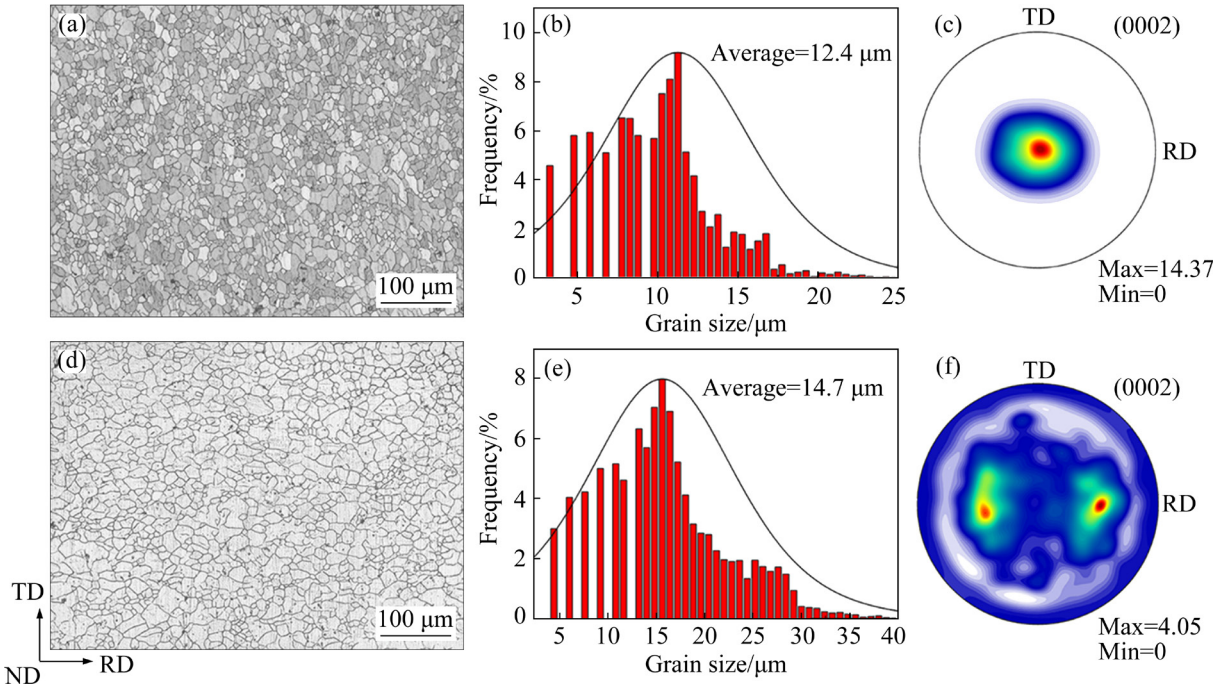

Fig. 1 Initial microstructure characteristics and texture of AZ31 magnesium alloy sheets with strong basal texture (a−c) and unusual double-peak texture (d−f): (a, d) Optical microstructure; (b, e) Statistical analysis of grain size; (c, f) (0002) pole figure

equiaxed and uniform grains shown in Figs. 1(a) and (d) occupy most of the microstructure, which confirms the occurrence of full recrystallization. Moreover, the correspondingly statistical analysis of grain size in Figs. 1(b) and (e) displays that both sheets are with similar grain size (the average grain size of 12.4 μm for sheet with strong basal texture and the average grain size of 14.7 μm for sheet with unusual double-peak texture). Therefore, effect of grain size on cold rolling formability and microstructure evolution of these two sheets can be excluded in the present study. With respect to the initial texture, Fig. 1(c) shows a strong basal texture where *c*-axis of most grains is almost parallel to ND. HUANG et al [21] and CHEN et al [19] also reported similar texture in AZ31 magnesium alloy sheet fabricated by hot rolling and annealing treatment. By comparison, Fig. 1(f) shows that sheet manufactured by ECAR−CB−A process is with a completely different non-basal texture, where basal poles tilt about ±40° away from ND to RD. SONG et al [11] concluded that this observed unusual double-peak texture has been rarely reported in AZ31 magnesium alloy sheet so far, let alone the relevant research on cold rolling formability.

3.2 Cold rolling formability of AZ31 magnesium alloy sheets

Figure 2 presents the appearance of cold rolled AZ31 magnesium alloy sheets and Table 2 displays the corresponding rolling parameters (sheet thickness per pass and reduction per pass) during multi-pass cold rolling process. It is obvious in Figure 2(a) that only after two passes of cold rolling, sheet with strong basal texture exhibits observable edge cracks and the correspondingly accumulated reduction is measured to be 18.3%. LI et al [22] reported similar result that under reduction per pass of ~8% at RT, AZ31 magnesium alloy sheet with strong basal texture can be rolled to ~20% until edge cracks occur. Both observations confirm that the rolling feasibility of AZ31 magnesium alloy sheet with strong basal texture is poor at RT. By comparison, edge cracks do not occur until five passes of cold rolling in sheet with unusual double-peak texture, as shown in Fig. 2(b). Correspondingly, the accumulated reduction achieves 39.2%, which is over twice as much as that in sheet with strong basal texture. Obviously, this unusual double-peak texture introduced by ECAR−CB−A process would contribute to a huge improvement on cold rolling formability of AZ31magnesium alloy sheet.

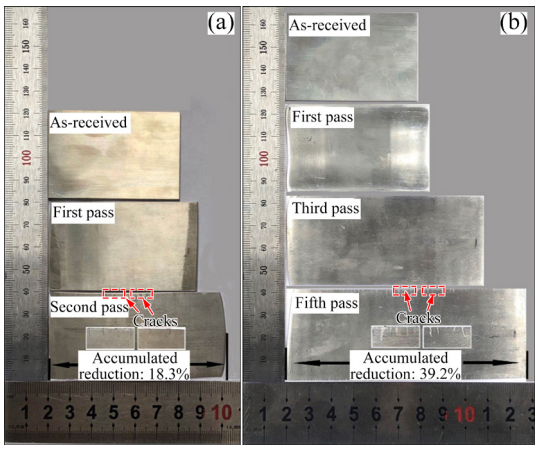

Fig. 2 Macrographs of AZ31 magnesium alloy sheets produced by multi-pass cold rolling process: (a) Sheet with strong basal texture; (b) Sheet with unusual double-peak texture

Table 2 Multi-pass cold rolling process for AZ31 magnesium alloy sheets

Material	Rolling pass	Thickness/mm	Reduction/%
Sheet with strong basal texture	1	1.10	8.30
	2	0.98	10.90
Sheet with unusual double-peak texture	1	1.08	10.00
	2	0.98	10.00
	3	0.89	9.20
	4	0.80	10.10
	5	0.73	8.80

3.3 Microstructure evolution during cold rolling

Figure 3 displays the deformed microstructure of AZ31 magnesium alloy sheets with strong basal texture and unusual double-peak texture after the first pass of cold rolling. As plastic strain is relatively small, grain morphology keeps nearly unchanged with equiaxed characteristic in both rolled sheets. Moreover, few twins exist in the microstructure of Fig. 3(a), while abundant twins with lamellar shape occur in Fig. 3(b). This issue could be further analyzed via EBSD investigations on these two rolled sheets, as shown in Fig. 4. Inverse pole figure (IPF) maps of Figs. 4(a) and (b) and grain boundary (GB) maps of Figs. 4(c) and (d)

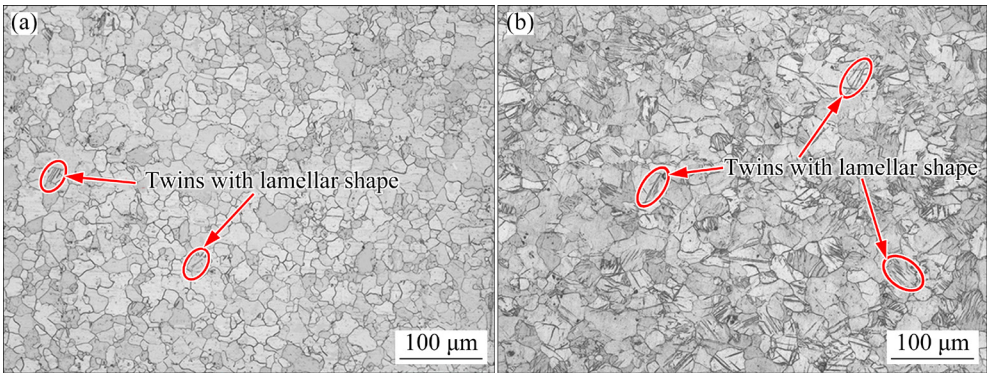

Fig. 3 Optical microstructure of AZ31 magnesium alloy sheets after the first pass of cold rolling: (a) Sheet with strong basal texture; (b) Sheet with unusual double-peak texture

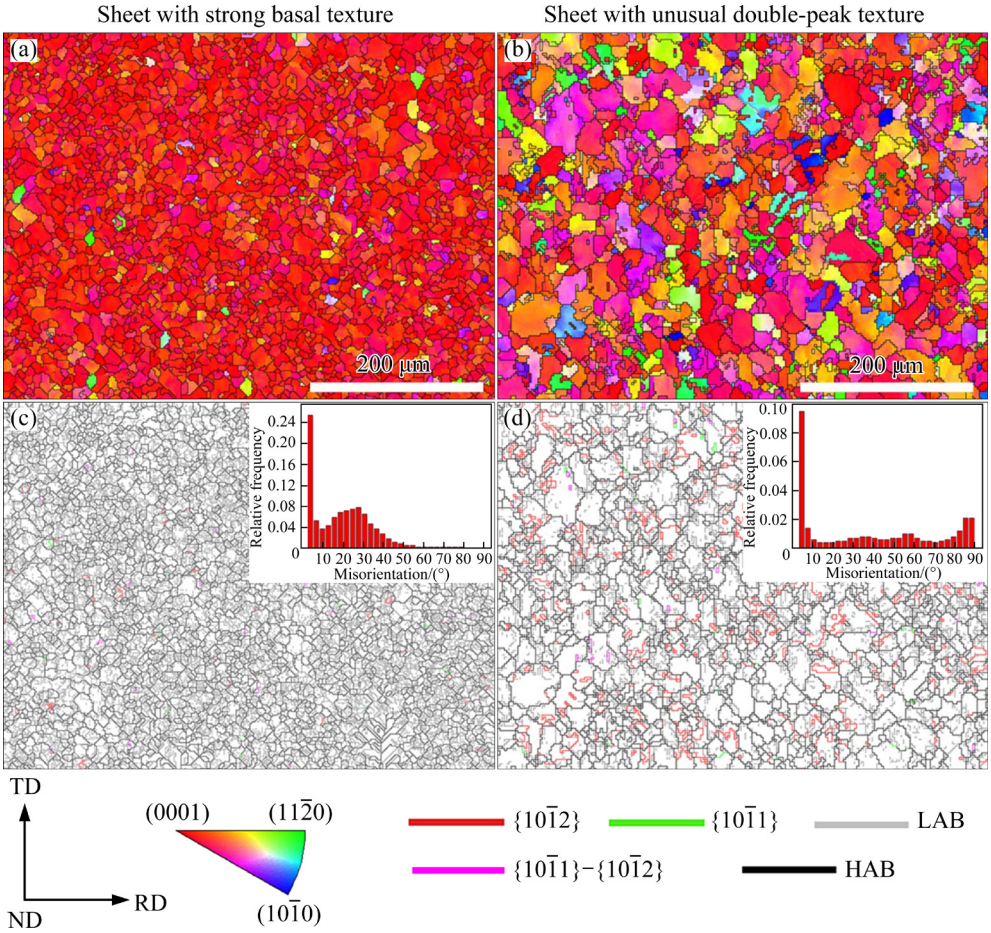

Fig. 4 EBSD patterns showing microstructure of AZ31 magnesium alloy sheets after the first pass of cold rolling: (a, b) IPF maps; (c, d) GB maps inserted with statistical analysis on misorientation distribution

collectively confirm that few $\{10\bar{1}2\}$ extension twins (ETs) ($86°\langle 1\bar{2}10\rangle \pm 5°$) appear within the deformed microstructure of rolled sheet with strong basal texture, let alone $\{10\bar{1}1\}$ compression twins (CTs) ($56°\langle 1\bar{2}10\rangle \pm 5°$) and $\{10\bar{1}1\}-\{10\bar{1}2\}$ secondary twins (STs) ($38°\langle 1\bar{2}10\rangle \pm 5°$), while $\{10\bar{1}2\}$ ETs occur frequently in the deformed microstructure of the rolled sheet with unusual double-peak texture. It has been generally accepted that $\{10\bar{1}2\}$ ET in AZ31 magnesium alloy prefers to sustain the elongation deformation along the *c*-axis of individual grains during the plastic deformation [1]. Although PANDEY et al [23] confirmed that $\{10\bar{1}2\}$ ET possesses the second-lowest critical resolved shear stress (CRSS) among all reported deformation mechanisms in AZ31

magnesium alloy, $\{10\bar{1}2\}$ ET can hardly be activated in sheet with strong basal texture during cold rolling process as there mainly exists compressive deformation along *c*-axis of individual grains. By comparison, as basal poles tilt about ±40° away from ND to RD in sheet with unusual double-peak texture, there will exist tensile deformation along *c*-axis of most individual grains during cold rolling process, contributing to the activation of $\{10\bar{1}2\}$ ET for the purpose of sustaining plastic strain. In addition, it is obvious that low angle boundary (LAB), whose misorientation is in the range of 2°−15°, occupies a larger portion of deformed microstructure in sheet with strong basal texture than that in sheet with unusual double-peak texture. HAN et al [24] reported that LAB is usually composed of dislocation during plastic deformation of AZ31 magnesium alloy. Therefore, the aforementioned observation indicates that dislocation slip is a dominant access to sustain plastic strain at the initial stage of cold rolling process in sheet with strong basal texture, while dislocation slip and $\{10\bar{1}2\}$ ET jointly and deeply participate in the plastic deformation of sheet with unusual double-peak texture.

With increasing the rolling pass, twins with lamellar shape appear within some grains of sheet with strong basal texture after the second pass of cold rolling, as shown in Fig. 5(a). CHANG et al [13] also reported this phenomenon in cold rolled AZ31 magnesium alloy sheet and they confirmed that these twins are identified to be $\{10\bar{1}2\}$ ETs. FERNÁNDEZ et al [25] reported that the activation of $\{10\bar{1}2\}$ ETs during cold rolling of AZ31 magnesium alloy sheet with strong basal texture should be mainly ascribed to the necessity of accommodating these local strains during plastic deformation. By comparison, the deformed microstructure in sheet with unusual double-peak texture is shown in Figs. 5(b) and (c). Obviously, $\{10\bar{1}2\}$ ETs occur nearly within each grain and they occupy a large portion of deformed microstructure. Moreover, $\{10\bar{1}2\}$ ETs intersect with each other in some grains. It should be mentioned that except for $\{10\bar{1}2\}$ ETs, other types of twins may also be activated here and this issue should be further analyzed by EBSD measurements on deformed sheets after the third pass and the fifth pass of cold rolling in the following section.

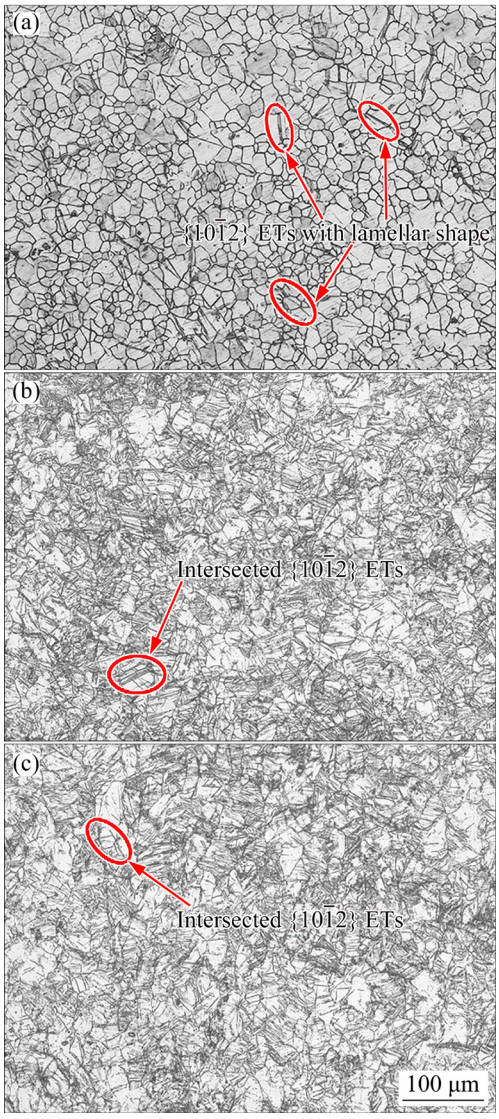

Fig. 5 Optical microstructure of AZ31 magnesium alloy sheets with strong basal texture (a) and unusual double-peak texture (b, c) at per-pass reduction of 10%: (a) The second pass; (b) The third pass; (c) The fifth pass

Figures 6 and 7 depict EBSD observations on rolled microstructure in sheet with unusual double-peak texture after the third pass and the fifth pass of cold rolling, separately. As deformation degree is relatively large, a minor step size of 0.5 μm and a small region with 114 μm in length and 86 μm in width were applied in the present study in order to confirm an acceptable indexing quality. IPF maps in Figs. 6(a) and 7(a) demonstrate that there exist twins with different morphologies. Further investigations by misorientation distribution, as shown in Figs. 6(b) and 7(b), demonstrate the occurrence of $\{10\bar{1}2\}$ ET, $\{10\bar{1}1\}$ CT and $\{10\bar{1}1\}-\{10\bar{1}2\}$ ST (peaks emerge at ~86°, ~56°

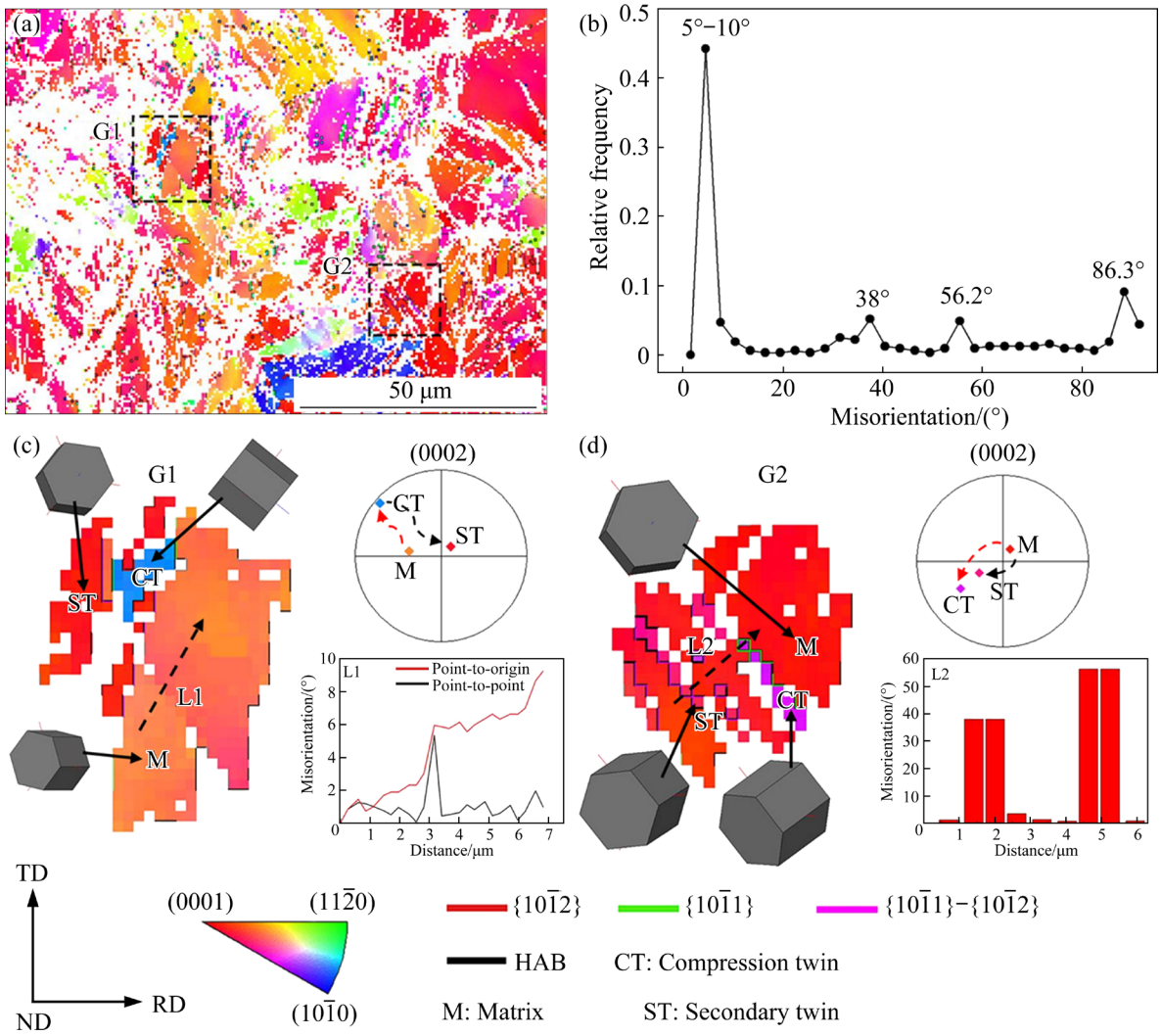

Fig. 6 EBSD characterization of deformed microstructure in sheet with unusual double-peak texture after the third pass of cold rolling: (a) IPF map; (b) Statistical analysis of misorientation distribution; (c, d) Twinning behavior of selected regions marked by black-dotted bordered rectangles in (a)

and ~38°, respectively). BARNETT et al [26] and AL-SAMMAN and GOTTSEIN [27] confirmed that $\{10\bar{1}1\}-\{10\bar{1}2\}$ ST is closely related to the formation of voids in magnesium alloys during plastic deformation at RT. Consequently, the emergence of $\{10\bar{1}1\}-\{10\bar{1}2\}$ ST indicates the weakening rolling capability about subsequent cold rolling process in sheet with unusual double-peak texture. For the purpose of specifically revealing the twinning behavior, two domains (G1 and G2) in Figs. 6(a) and 7(a) were selected and analyzed from different perspectives. The maximum values for point-to-point misorientation and point-to-origin misorientation in line L1 are ~5.4° and ~9.3° in Fig. 6(c), while the corresponding values are ~3.2° and ~15.8° in Fig. 7(c). This observation indicates that within the grain of matrix, dislocation slip serves as an indispensable mechanism to sustain plastic strain and it contributes to the formation of LAB. Misorientation analysis along L2 line in Figs. 6(d) and 7(d) further verifies the formation of $\{10\bar{1}1\}$ CT and/or $\{10\bar{1}1\}-\{10\bar{1}2\}$ ST. In addition, it is clear in Figs. 6(c, d) and Figs. 7(c, d) that $\{10\bar{1}1\}$ CT trends to rotate its initial orientation away from ND, while $\{10\bar{1}1\}-\{10\bar{1}2\}$ ST prefers to rotate its initial orientation towards ND.

3.4 Texture evolution during cold rolling

The texture evolution of AZ31 magnesium alloy sheets with strong basal texture and unusual double-peak texture during cold rolling process is depicted via (0002) and (10$\bar{1}$0) pole figures in

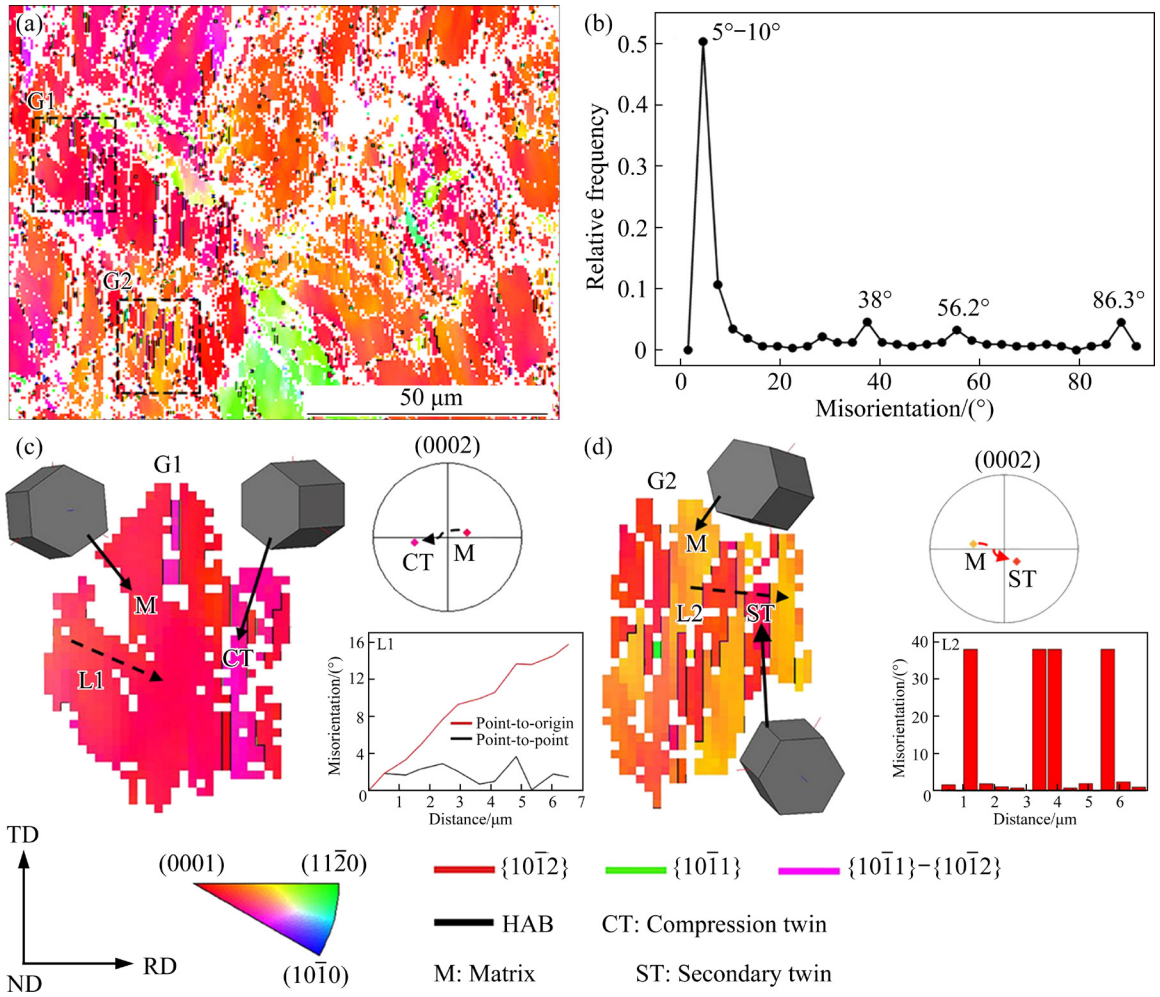

Fig. 7 EBSD characterization of deformed microstructure in sheet with unusual double-peak texture after the fifth pass of cold rolling: (a) IPF map; (b) Statistical analysis of misorientation distribution; (c, d) Twinning behavior of selected regions marked by black-dotted bordered rectangles in (a)

Fig. 8. It is obvious in Figs. 8(a) and (c) that cold rolling contributes to the tilting of *c*-axis of some grains away from ND to RD, which results in the ellipsoidal distribution of basal texture intensity in (0002) pole figures. STYCZYNSKI et al [28] and ZHANG et al [29] also reported this texture characteristic in cold rolled AZ31 magnesium alloy sheet. Moreover, cold rolling mainly causes the concentration of tilted basal poles towards ND with increasing the plastic deformation, as shown in Figs. 8(b), (d) and (e). Obviously, the tendency about concentration of tilted basal poles towards ND is relatively remarkable from the first pass to the third pass, while the tendency about the concentration of tilted basal poles towards ND is barely detectable from the third pass to the fifth pass. The underlying mechanisms resulting in this phenomenon will be discussed in the following section.

4 Discussion

CHUN and DAVIES [16] and WANG et al [30] both reported that the initial texture shows a great impact on microstructure characteristics and texture evolution of AZ31 magnesium alloy sheet during cold rolling process. It can affect the activities of various slip/twining modes, which further determines the cold rolling formability of AZ31 magnesium alloy sheet. Therefore, in order to illuminate the underlying mechanisms leading to the superior cold rolling formability of AZ31 magnesium alloy sheet with unusual double-peak texture, the effect of this special non-basal texture on activation of various slip/twining modes during cold rolling process should be deeply analyzed. STYCZYNSKI et al [28] and KUANG et al [10] reported that the deformation mechanisms during cold rolling process of AZ31

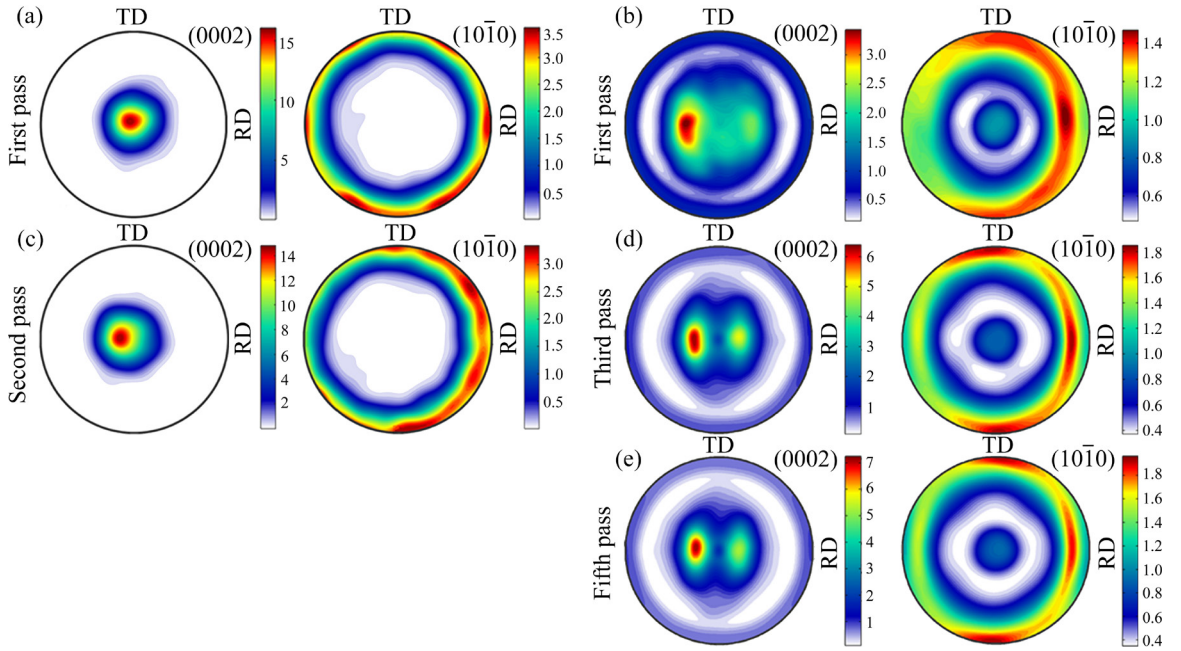

Fig. 8 (0002) and (10$\bar{1}$0) pole figures of AZ31 magnesium alloy sheets during multi-pass cold rolling process: (a, c) Sheet with strong basal texture; (b, d, e) Sheet with unusual double-peak texture

magnesium alloy sheet mainly include basal ⟨*a*⟩ slip, prismatic ⟨*a*⟩ slip, pyramidal ⟨*c*+*a*⟩ slip and {10$\bar{1}$2} ET. To intuitively elucidate the effect of texture characteristics on the activation of these involved slip/twinning modes, Schmid factor (SF) analysis is applied during the cold rolling process of AZ31 magnesium alloy sheet. The calculation of effective SF during rolling can be realized via the following equation [31,32]:

$$\mathrm{SF}_{\text{rolling}} = \frac{\left(\cos\phi_{\mathrm{RD}}\cos\varphi_{\mathrm{RD}} - \cos\phi_{\mathrm{ND}}\cos\varphi_{\mathrm{ND}}\right)}{2}.$$

where ϕ_{RD} and ϕ_{ND} refer to the angles between the normal direction of slip/twining plane and RD, ND, respectively. φ_{RD} and φ_{ND} represent the angles between the slip/twining direction and RD, ND, respectively. Accordingly, the distribution of $\mathrm{SF}_{\text{rolling}}$ for basal ⟨*a*⟩ slip, prismatic ⟨*a*⟩ slip, pyramidal ⟨*c*+*a*⟩ slip and {10$\bar{1}$2} ET can be realized and visualized by coding in MATLAB, as shown in Fig. 9. It is worth noting that due to the polar nature of {10$\bar{1}$2} ET, the scope of $\mathrm{SF}_{\text{rolling}}$ changes from −0.5 to 0.5, while the corresponding scope for dislocation mode varies from 0 to 0.5.

Figure 9(a) displays that $\mathrm{SF}_{\text{rolling}}$ for basal ⟨*a*⟩ slip in sheet with strong basal texture (0−0.2) is distinctively smaller than the one in sheet with unusual double-peak texture (0.3−0.5). This observation indicates that at the beginning of cold

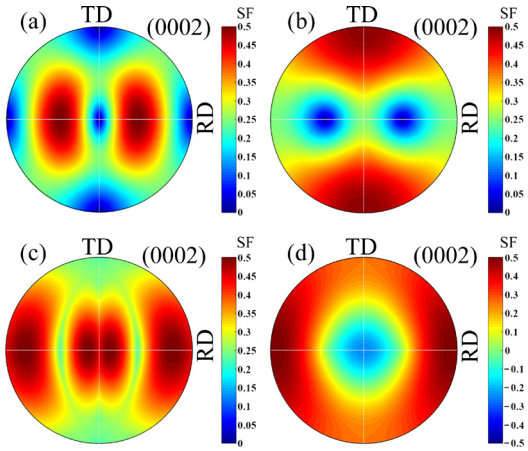

Fig. 9 Distribution of effective SF for various deformation mechanisms in AZ31 magnesium alloy sheet undergoing cold rolling along ND: (a) Basal ⟨*a*⟩ slip; (b) Prismatic ⟨*a*⟩ slip; (c) Pyramidal ⟨*c*+*a*⟩ slip; (d) {10$\bar{1}$2} ET

rolling process, basal ⟨*a*⟩ slip could be activated more easily in sheet with unusual double-peak texture. Although there exists a concentration tendency of tilted basal poles towards ND during cold rolling process, as shown in Figs. 8(b), (d) and (e), $\mathrm{SF}_{\text{rolling}}$ for basal ⟨*a*⟩ slip in sheet with unusual double-peak texture is always larger than the one in sheet with strong basal texture. In addition, Figs. 9(b) and (c) show that $\mathrm{SF}_{\text{rolling}}$ for prismatic ⟨*a*⟩ slip (0.2−0.3) and $\mathrm{SF}_{\text{rolling}}$ for pyramidal ⟨*c*+*a*⟩ slip (0.4−0.5) in sheet with strong basal texture are

apparently larger than the corresponding ones (prismatic ⟨*a*⟩ slip (0−0.2) and pyramidal ⟨*c*+*a*⟩ slip (0.25−0.45)) in sheet with unusual double-peak texture. This observation indicates that at the initiation of cold rolling, it is even harder to start prismatic ⟨*a*⟩ slip and pyramidal ⟨*c*+*a*⟩ slip in sheet with unusual double-peak texture. Based on the texture evolution in Fig. 8, it is clear that sheet with strong basal texture always possesses relatively large $SF_{rolling}$ for prismatic ⟨*a*⟩ slip and pyramidal ⟨*c*+*a*⟩ slip during cold rolling process. With respect to $\{10\bar{1}2\}$ ET, Fig. 9(d) confirms that $SF_{rolling}$ in sheet with strong basal texture is obviously in a low level (from −0.5 to 0.1), while $SF_{rolling}$ in sheet with unusual double-peak texture mainly varies from 0.1 to 0.3. This observation demonstrates that $\{10\bar{1}2\}$ ET could emerge more frequently in sheet with unusual double-peak texture. This issue coincides well with the microstructure characteristics shown in Fig. 4.

Based on the aforementioned SF analysis and the corresponding microstructure characterization, mechanisms for sustaining plastic strain in AZ31 magnesium alloy sheets during cold rolling process can be concluded and displayed in Fig. 10. PANDEY et al [23] reported that basal ⟨*a*⟩ slip possesses the lowest CRSS among all involved deformation mechanisms (basal ⟨*a*⟩ slip < $\{10\bar{1}2\}$ ET < prismatic ⟨*a*⟩ slip < pyramidal ⟨*c*+*a*⟩ slip) and it is the first candidate for sustaining plastic strain during plastic deformation of magnesium alloys. Therefore, although $SF_{rolling}$ for basal ⟨*a*⟩ slip is relatively small among all involved dislocation modes, it can still be termed as the main deformation mechanism for sheet with strong basal texture during cold rolling process, as shown in Figs. 10(a) and (c). In addition, although prismatic ⟨*a*⟩ slip and pyramidal ⟨*c*+*a*⟩ slip possess high CRSS, they can be activated due to their relatively large $SF_{rolling}$ for sheet with strong basal texture. STYCZYNSKI et al [28] and LIAN et al [33] reported that pyramidal ⟨*c*+*a*⟩ slip can be termed as a "compatibility first" deformation mechanism in AZ31 magnesium alloy during plastic deformation and its activity is related to the tilting of basal pole away from ND. Therefore, the texture characteristics shown in Figs. 8(a) and (c) would not be obtained without the assistance of this deformation mechanism (Figs. 10(a) and (c)). With respect to sheet with unusual double-peak texture, the relatively large $SF_{rolling}$ values for basal ⟨*a*⟩ slip and $\{10\bar{1}2\}$ ET indicate a massive activity during cold rolling process, as shown in Figs. 10(b) and (d). KABIRIAN et al [1] and PANDEY et al [23] confirmed that their large activation contributes to enhancing plasticity of magnesium alloy. Consequently, the superior cold rolling formability in sheet with unusual double-peak texture can be obtained with the assistance of basal ⟨*a*⟩ slip and $\{10\bar{1}2\}$ ET.

Besides, LIU et al [34] and CHEN et al [19] reported that there exist six variants (V1 to V6) of $\{10\bar{1}2\}$ ET in magnesium alloys and the selective activation of $\{10\bar{1}2\}$ ET variants deeply affects the microstructure characteristics and the texture evolution during plastic deformation. To

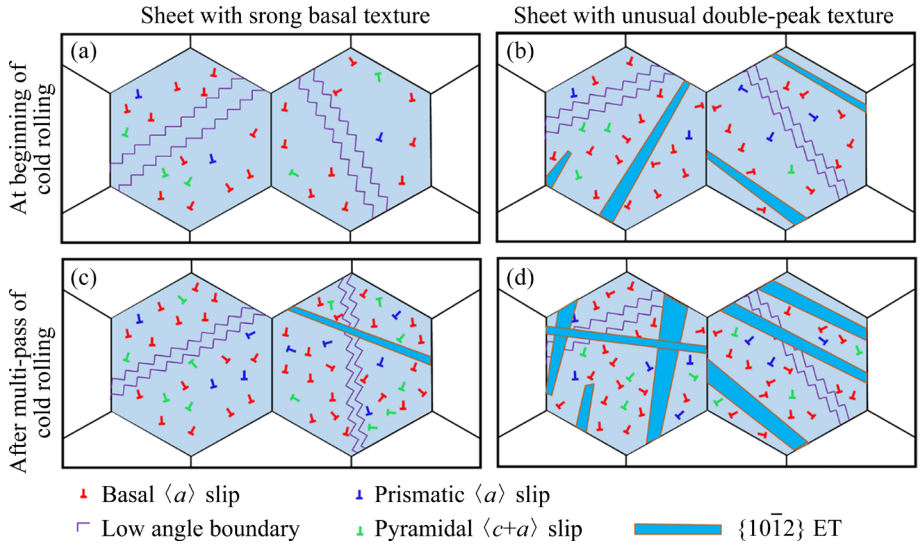

Fig. 10 Mechanism illustration for AZ31 magnesium alloy sheets with strong basal texture and unusual double-peak texture during cold rolling process

better understand the twinning behavior and explain the relationship between grain orientation and the activated $\{10\bar{1}2\}$ ET variants in sheet with unusual double-peak texture after the first pass of cold rolling, twelve grains are artificially selected from Fig. 4(b). They are thereafter analyzed from different perspectives, as shown in Fig. 11, which contains the IPF maps, (0002) pole figures and twin variants maps. The determination of twin variant is collectively conducted by means of trace method and SF analysis. The corresponding SF of each theoretical $\{10\bar{1}2\}$ ET variant in selected grains is shown in Table 3. Actually, these selected twelve grains can be further divided into three groups by the tilted angle between *c*-axis of grains and ND, namely Grains 1−3 with the tilted angle less than

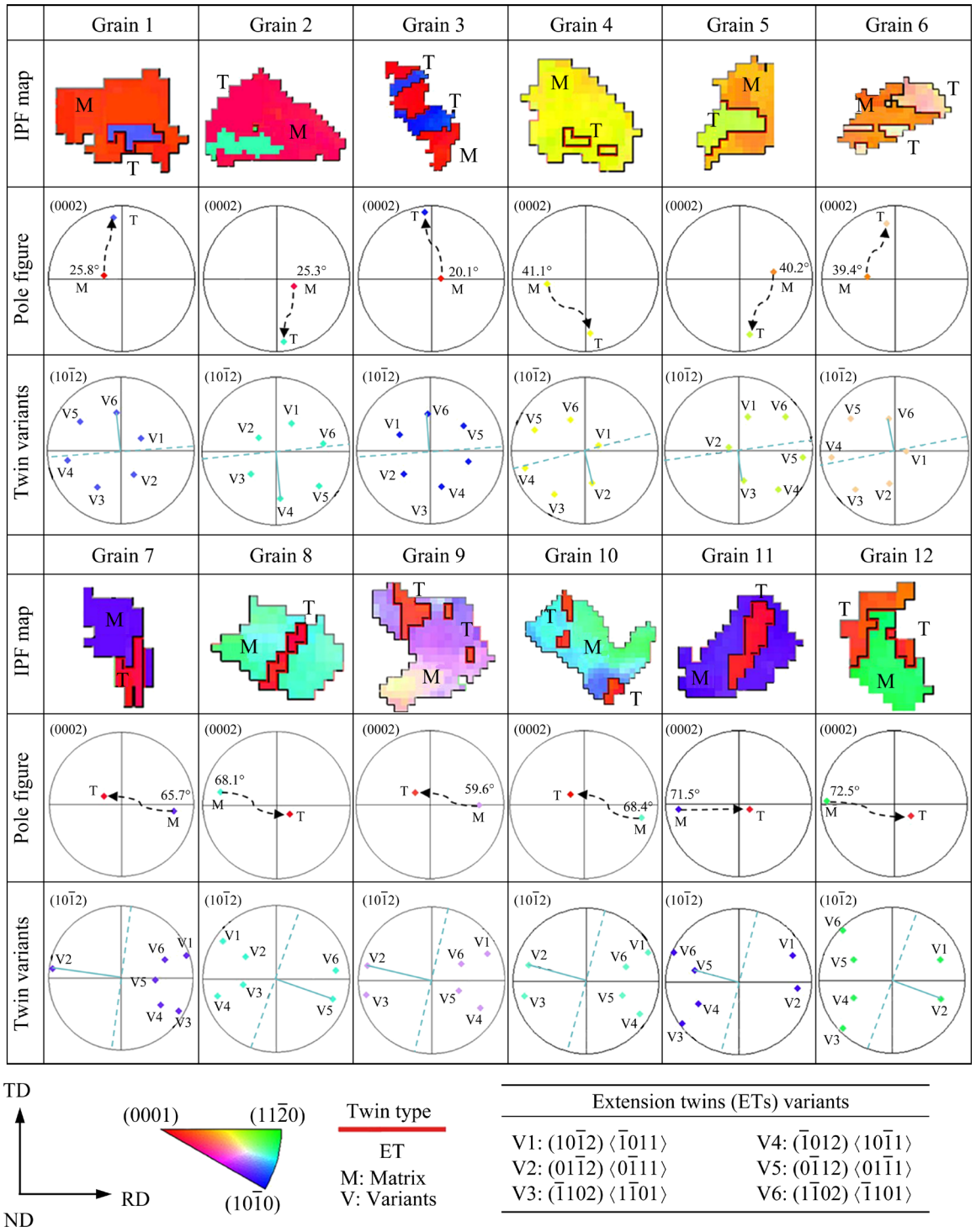

Fig. 11 IPF maps, (0002) pole figures and twin variants maps for selected grains in AZ31 magnesium alloy sheet with unusual double-peak texture after the first pass of cold rolling

Table 3 SF values of theoretical $\{10\bar{1}2\}$ ET variants of selected grains in Fig. 4(b)

Grain No.	SF						Activated variant
	V1	V2	V3	V4	V5	V6	
1	−0.45	−0.35	−0.24	−0.42	−0.32	−0.24	V6
2	−0.19	−0.29	−0.38	−0.20	−0.32	−0.41	V4
3	−0.30	−0.47	−0.29	−0.31	−0.49	−0.30	V6
4	−0.18	0.06	−0.10	−0.20	0.08	−0.04	V2
5	−0.12	−0.17	−0.07	−0.14	−0.23	−0.11	V3
6	−0.14	−0.22	−0.09	−0.12	−0.16	−0.06	V6
7	0.22	0.37	0.23	0.21	0.32	0.20	V2
8	−0.01	0.21	−0.21	−0.03	0.20	−0.20	V5
9	−0.25	0.13	−0.11	−0.27	0.10	−0.12	V2
10	−0.23	0.18	−0.02	−0.23	0.20	−0.01	V2
11	−0.04	0.21	−0.16	−0.04	0.24	−0.13	V5
12	−0.23	0.18	0.07	−0.22	0.18	0.06	V2

40°, Grains 4−6 with the tilted angle about 40° and Grains 7−12 with the tilted angle more than 40°. It is worth noting that only one $\{10\bar{1}2\}$ ET variant could be activated in these selected grains, as shown in Fig. 10. Moreover, when *c*-axis of grain tilts less than or about 40° to ND, the activated $\{10\bar{1}2\}$ ET will mostly rotate its initial orientation to about TD. By comparison, when *c*-axis of grain tilts more than 40° to ND, the activated $\{10\bar{1}2\}$ ET will dominantly rotate its initial orientation to about ND. As Fig. 1(f) shows that the tilted angles between most of *c*-axis of grains and ND are larger than 40° in sheet with unusual double-peak texture, there is no doubt that these activated $\{10\bar{1}2\}$ ET variants mainly contribute to the concentration of tilted basal poles towards ND at early stage of cold rolling process. With increasing the plastic strain, $SF_{rolling}$ for $\{10\bar{1}2\}$ ET as well as its activity decreases remarkably. Consequently, the tendency about the concentration of tilted basal poles towards ND is weakened.

5 Conclusions

(1) An unusual double-peak texture is introduced in AZ31 magnesium alloy sheet by a novel ECAR−CB−A process. Its microstructure characteristics and texture evolution during cold rolling process are systematically investigated via experimental observations based on OM and EBSD measurements, and compared with those in sheet strong basal texture.

(2) Under the condition of 10% reduction per pass, the accumulated reduction in sheet with unusual double-peak texture is as high as 39.2%, which is over twice as much as that (18.3%) in sheet with strong basal texture.

(3) $\{10\bar{1}2\}$ ETs rarely occur in sheet with strong basal texture during cold rolling process unless there is need for accommodating local strains between individual grains. By comparison, the amount of $\{10\bar{1}2\}$ ETs increases with increasing the rolling pass. Moreover, only one variant is mainly activated for each $\{10\bar{1}2\}$ ET in grains of sheet with unusual double-peak texture, which mainly rotates its initial grain orientation to about ND during cold rolling process. This issue finally results in the concentration of tilted basal poles.

(4) Sheet with unusual double-peak texture possesses obviously large SF values for basal $\langle a\rangle$ slip and $\{10\bar{1}2\}$ ET, which leads to extensive activities of these two deformation mechanisms to sustain plastic strain during cold rolling process. This issue is responsible for the superior cold rolling formability of sheet with unusual double-peak texture.

Acknowledgments

This work was supported by the Fund for Distinguished Young Scholars of China Academy of Space Technology (No. 2021399), the National Natural Science Foundation of China (No. 51805064), and the Science and Technology Research Program of Chongqing Municipal Education Commission, China (No. KJQN202101141).

References

[1] KABIRIAN F, KHAN A S, GNÄUPEL-HERLOD T. Visco-plastic modeling of mechanical responses and texture evolution in extruded AZ31 magnesium alloy for various loading conditions [J]. International Journal of Plasticity, 2015, 68: 1−20.

[2] SONG Jiang-feng, SHE Jia, CHEN Dao-lun, PAN Fu-sheng. Latest research advances on magnesium and magnesium alloys worldwide [J]. Journal of Magnesium and Alloys, 2020, 8(1): 1−41.

[3] LIANG Min-jie, ZHENG Jie, LIU Huan, YAO Bao-xing. Microstructure and mechanical properties of AZ31 alloy prepared by cyclic expansion extrusion with asymmetrical extrusion cavity [J]. Transactions of Nonferrous Metals Society of China, 2022, 32(1): 122−133.

[4] ABBASI M, BAGHERI B, SHARIFI F. Simulation and experimental study of dynamic recrystallization process during friction stir vibration welding of magnesium alloys [J]. Transactions of Nonferrous Metals Society of China, 2021, 31(9): 2626−2650.

[5] KANG D H, KIM D W, KIM S, BAE G T, KIM K H, KIM N J. Relationship between stretch formability and work-hardening capacity of twin-roll cast Mg alloys at room temperature [J]. Scripta Materialia, 2009, 61(7): 768−771.

[6] YANG Qing-shan, JIANG Bin, ZHOU Guan-yu, DAI Jia-hong, PAN Fu-sheng. Influence of an asymmetric shear deformation on microstructure evolution and mechanical behavior of AZ31 magnesium alloy sheet [J]. Materials Science and Engineering: A, 2014, 590: 440−447.

[7] WANG Ye, LI Feng, LI Xue-wen, FANG Wen-bin. Unusual texture formation and mechanical property in AZ31 magnesium alloy sheets processed by CVCDE [J]. Journal of Materials Processing Technology, 2020, 275: 116360.

[8] HUANG Xin-sheng, SUZUKI K, WATAZU A, SHIGEMATSU I, SAITO N. Microstructure and texture of Mg−Al−Zn alloy processed by differential speed rolling [J]. Journal of Alloys and Compounds, 2008, 457(1/2): 408−412.

[9] LEE J H, LEE J U, KIM S H, SONG S W, LEE C S, PARK S H. Dynamic recrystallization behavior and microstructural evolution of Mg alloy AZ31 through high-speed rolling [J]. Journal of Materials Science & Technology, 2018, 34(10): 1747−1755.

[10] KUANG J, LOW T S E, NIEZGODA S R, LI X H, GENG Y B, LUO A A, TANG G Y. Abnormal texture development in magnesium alloy Mg−3Al−1Zn during large strain electroplastic rolling: Effect of pulsed electric current [J]. International Journal of Plasticity, 2016, 87: 86−99.

[11] SONG Deng-hui, ZHOU Tao, TU Jian, SHI Lai-xin, SONG Bo, HU Li, YANG Ming-bo, CHEN Qiang, LU Li-wei. Improved stretch formability of AZ31 sheet via texture control by introducing a continuous bending channel into equal channel angular rolling [J]. Journal of Materials Processing Technology, 2018, 259: 380−386.

[12] HE Jun-jie, MAO Yong, FU Ying-jie, JIANG Bin, XIONG Kai, ZHANG Shun-meng, PAN Fu-sheng. Improving the room-temperature formability of Mg−3Al−1Zn alloy sheet by introducing an orthogonal four-peak texture [J]. Journal of Alloys and Compounds, 2019, 797: 443−455.

[13] CHANG L L, SHANG E F, WANG Y N, ZHAO X, QI M. Texture and microstructure evolution in cold rolled AZ31 magnesium alloy [J]. Materials Characterization, 2009, 60(6): 487−491.

[14] LEE S W, KIM S H, PARK S H. Microstructural characteristics of AZ31 alloys rolled at room and cryogenic temperatures and their variation during annealing [J]. Journal of Magnesium and Alloys, 2020, 8(2): 537−545.

[15] HUANG Guang-sheng, XU Wei, HUANG Guang-jie, WANG Ling-yun. Microstructure and mechanical properties of AZ31B magnesium alloy after cold rolling and annealing [J]. Heat Treatment of Metals, 2009, 34(5): 18−20.

[16] CHUN Y B, DAVIES C H J. Texture effects on development of shear bands in rolled AZ31 alloy [J]. Materials Science and Engineering: A, 2012, 556: 253−259.

[17] LEE S W, HAN G K, JUN T S, PARK S H. Effects of initial texture on deformation behavior during cold rolling and static recrystallization during subsequent annealing of AZ31 alloy [J]. Journal of Materials Science & Technology, 2021, 66: 139−149.

[18] TU Jian, ZHOU Tao, LIU Lei, SHI Lai-xin, HU Li, SONG Deng-hui, SONG Bo, YANG Ming-bo, CHEN Qiang, PAN Fu-sheng. Effect of rolling speeds on texture modification and mechanical properties of the AZ31 sheet by a combination of equal channel angular rolling and continuous bending at high temperature [J]. Journal of Alloys and Compounds, 2018, 768: 598−607.

[19] CHEN Yu, HU Li, SHI Lai-xin, ZHOU Tao, TU Jian, CHEN Qiang, YANG Ming-bo. Effect of texture types on microstructure evolution and mechanical properties of AZ31 magnesium alloy undergoing uniaxial tension deformation at room temperature [J]. Materials Science and Engineering: A, 2020, 769: 138497.

[20] HIELSCHER R, SCHAEBEN H. A novel pole figure inversion method: Specification of the MTEX algorithm [J]. Journal of Applied Crystallography, 2008, 41(6): 1024−1037.

[21] HUANG Xin-sheng, CHINO Y, MABUCHI M, MATSUDA M. Influences of grain size on mechanical properties and cold formability of Mg−3Al−1Zn alloy sheets with similar weak initial textures [J]. Materials Science and Engineering: A, 2014, 611: 152−161.

[22] LI Miao-miao, WU Bao-lin, ZHANG Li, WAN Gang, DU Xing-hao. Effects of multi-pass rolling reduction on deformability of AZ31 magnesium alloy sheet [J]. Hot Working Technology, 2017, 46(4): 38−41.

[23] PANDEY A, KABIRIAN F, HWANG J H, CHOI S H, KHAN A S. Mechanical responses and deformation mechanisms of an AZ31 Mg alloy sheet under dynamic and simple shear deformations [J]. International Journal of Plasticity, 2015, 68: 111−131.

[24] HAN Ting-zhuang, HUANG Guang-sheng, WANG You-gen, WANG Guang-gang, ZHAO Yan-chun, PAN Fu-sheng. Enhanced mechanical properties of AZ31 magnesium alloy sheets by continuous bending process after V-bending [J]. Progress in Natural Science: Materials International, 2016, 26(1): 97−102.

[25] FERNÁNDEZ A, JÉRUSALEM A, GUTIÉRREZ-URRUTIA I, PÉREZ-PRADO M T. Three-dimensional investigation of grain boundary–twin interactions in a Mg AZ31 alloy by electron backscatter diffraction and continuum modeling [J]. Acta Materialia, 2013, 61(20): 7679−7692.

[26] BARNETT M R, KESHAVARZ Z, BEER A G, ATWELL D. Influence of grain size on the compressive deformation of wrought Mg−3Al−1Zn [J]. Acta Materialia, 2004, 52(17): 5093−5103.

[27] AL-SAMMAN T, GOTTSTEIN G. Room temperature formability of a magnesium AZ31 alloy: Examining the role of texture on the deformation mechanisms [J]. Materials Science and Engineering: A, 2008, 488(1/2): 406−414.

[28] STYCZYNSKI A, HARTIG C, BOHLEN J, LETZIG D. Cold rolling textures in AZ31 wrought magnesium alloy [J]. Scripta Materialia, 2004, 50(7): 943−947.

[29] ZHANG Hua, CHENG Wei-li, FAN Jian-feng, XU Bing-she, DONG Hong-biao. Improved mechanical properties of AZ31 magnesium alloy sheets by repeated cold rolling and annealing using a small pass reduction [J]. Materials Science and Engineering: A, 2015, 637: 243−250.

[30] WANG X J, XU D K, WU R Z, CHEN X B, PENG Q M, JIN L, XIN Y C, ZHANG Z Q, LIU Y, CHEN X H, CHEN G, DENG K K, WANG H Y. What is going on in magnesium alloys? [J]. Journal of Materials Science & Technology, 2018, 34(2): 245−247.

[31] SHAO Jian-bo, CHEN Zhi-yong, CHEN Tao, LIU Chu-ming. Deformation mechanism of Mg−Gd−Y−Zn−Zr alloy containing long-period stacking ordered phases during hot rolling [J]. Metallurgical and Materials Transactions A, 2020, 51(4): 1911−1923.

[32] LUO J R, GODFREY A, LIU W, LIU Q. Twinning behavior of a strongly basal textured AZ31 Mg alloy during warm rolling [J]. Acta Materialia, 2012, 60(5): 1986−1998.

[33] LIAN Yong, HU Li, ZHOU Tao, YANG Ming-bo, ZHANG Jin. Numerical investigation of secondary deformation mechanisms on plastic deformation of AZ31 magnesium alloy using viscoplastic self-consistent model [J]. Metals, 2019, 9(1): 41.

[34] LIU Guang-dong, XIN Ren-long, SHU Xiao-gang, WANG Chun-peng, LIU Qing. The mechanism of twinning activation and variant selection in magnesium alloys dominated by slip deformation [J]. Journal of Alloys and Compounds, 2016, 687: 352−359.

罕见双峰织构在提高 AZ31 镁合金板材冷轧成形性能中的作用

韩修柱[1]，胡 励[2]，贾东永[1]，陈家明[2]，周 涛[2]，江树勇[3]，田 政[1]

1. 北京空间飞行器总体设计部，北京 100094；
2. 重庆理工大学 材料科学与工程学院，重庆 400054；
3. 太原理工大学 材料科学与工程学院，太原 030024

摘 要：对基极由板材法向向轧向偏离±40°的罕见双峰织构 AZ31 镁合金板材进行多道次冷轧实验研究。该板材由等径角轧制−连续弯曲−退火工艺制备。实验结果表明，该罕见双峰织构能大幅度提高板材的冷轧累积减薄率至 39.2%，是传统强基面织构板材冷轧累积减薄率的 2 倍以上(18.3%)。金相和电子背散射衍射分析表明，该罕见双峰织构板材在冷轧过程中的显微组织及织构演化与传统强基面织构板材的区别显著。施密特因子(SF)分析表明，在冷轧过程中，基面⟨*a*⟩滑移和 $\{10\bar{1}2\}$ 拉伸孪晶的 SF 值较大，而柱面⟨*a*⟩滑移和锥面⟨*c*+*a*⟩滑移的 SF 值较小。因此，基面⟨*a*⟩滑移和 $\{10\bar{1}2\}$ 拉伸孪晶在该罕见双峰织构 AZ31 镁合金板材冷轧过程中将被大量激活来承载塑性应变，进而显著提高板材的冷轧成形性能。

关键词：AZ31 镁合金；非基面织构；冷轧工艺；显微组织演化；变形机制

(Edited by Wei-ping CHEN)